Magnetic and vibrational Raman scattering from II-VI magnetic quantum wells: ZnTe/$Cd_{1-x}Mn_xSe$ and ZnTe/MnSe

Eunsoon Oh and A. K. Ramdas
Department of Physics, Purdue University, West Lafayette, Indiana 47907-1301

N. Samarth, H. Luo, and J. K. Furdyna
Department of Physics, University of Notre Dame, Notre Dame, Indiana 46556
(Received 15 October 1992)

In a type-II multiple quantum well consisting of ZnTe/$Cd_{1-x}Mn_xSe$, the Raman shifts associated with the spin flip of donor-bound electrons in the $Cd_{1-x}Mn_xSe$ wells are significantly smaller than in bulk $Cd_{1-x}Mn_xSe$ of comparable x. This effect is ascribed to the decrease in the effective Mn^{2+} concentration as a result of the penetration of the donor electron wave function into the nonmagnetic barrier. Raman electron paramagnetic resonance of Mn^{2+} is also observed in these type-II quantum wells, whose resonance enhancement is associated with spatially direct interband transitions from states above the barrier for holes to the quantum confined electronic states. We also report the observation of confined longitudinal-optical phonons and folded acoustic phonons in strained ZnTe/MnSe multiple quantum wells. In this heterostructure we observe an unusual combination mode involving vibrational excitations in *two* different layers (ZnTe and MnSe).

I. INTRODUCTION

While quantum-well structures and superlattices involving wide-gap II-VI semiconductors have a special appeal in the quest for diode injection lasers in the blue and the blue-green,[1] many general physical issues associated with them need to be fully understood. For example, the lattice mismatch and its consequences, such as the heavy- and light-hole splitting, and the nature of the band alignment leading to a type-I or a type-II quantum-well structure, have to be addressed both experimentally and theoretically. The wave functions of the confined states for electrons and holes offer important insights into these questions.

II-VI diluted magnetic semiconductors (DMS's) are ternary compounds, where some of the group-II elements are replaced by magnetic ions, such as Mn^{2+}. The spin-spin exchange interaction between band electrons and magnetic ions in DMS's results in a huge excitonic Zeeman splitting. DMS's thus provide an interesting opportunity to study spin systems and, in particular, DMS-based quantum-well structures allow the investigation of exchange-related phenomena in the context of reduced dimensionality. Among these, a recent study shows that ZnTe/$Cd_{1-x}Mn_xSe$ quantum wells possess certain unique characteristics which can be understood in terms of a type-II band alignment, where electrons are localized in the magnetic wells ($Cd_{1-x}Mn_xSe$), spatially separated from holes, which are confined to nonmagnetic ZnTe layers.[2] For example, the spatially indirect transitions between the valence-band maximum of ZnTe and the conduction-band minimum of $Cd_{1-x}Mn_xSe$ are expected to occur *below* the energy gap of $Cd_{1-x}Mn_xSe$—indeed a strong photoluminescence *is* observed in the *infrared*. Absorption spectra in the *visible* range also reveal a strong transition, with large Zeeman splittings as in the bulk, whereas only a very weak and broad photoluminescence corresponding to this absorption feature is observed. The absorption feature is attributed to the transition from states above the barrier for holes to confined electronic states in the well, the transition being *spatially direct*. It is well known that the magnetic excitations as observed in Raman scattering (such as spin-flip transitions within the Zeeman multiplets or the spin-flip of the donor-bound electrons) are mediated by interband transitions.[3] Since donor-bound magnetic polarons are observed in these type-II quantum wells,[4] one can study the enhancement of the Raman scattering associated with the spin flip of the donor-bound electrons near such interband transitions.

Another type of question arises in the context of the reduced dimensionality. One could ask how the effective Mn^{2+} concentration ("seen" by electrons) depends on the confinement of the electron wave function, how the exchange interaction between the holes and the Mn^{2+} ions is influenced by the spatial separation, and how the antiferromagnetic interaction between Mn^{2+} ions themselves is affected. Useful information about the wave functions for confined electrons or holes can be obtained from photoluminescence and the spin-flip Raman shift of the donor-bound electrons in the superlattices where either the well or the barrier is a DMS. The magnitude of the Zeeman shift in the photoluminescence in $Zn_{1-x}Cd_xSe/Zn_{1-y}Mn_ySe$ (Ref. 5) and the Raman shift associated with the spin flip of the donor-bound electrons in $Cd_{1-x}Mn_xTe$/ CdTe can be understood in terms of the wave-function penetration into the magnetic barrier,[6] as manifested by the larger associated effects for the smaller well widths. The study of the spin-flip Raman scattering in a ZnTe/$Cd_{1-x}Mn_xSe$ type-II multiple quantum well

 ©1993 The American Physical Society

(MQW) is of interest in that it represents an opposite situation, where the DMS constitutes *a well for electrons but a barrier for holes.*

We have studied the spin-flip Raman scattering of donor-bound electrons in order to obtain an insight into the effect of the lower dimensionality which, in turn, controls the "effective" manganese concentration probed by the quantum confined electronic levels. We also have studied the longitudinal-optical phonon in these MQW's; the lattice mismatch between ZnTe and $Cd_{1-x}Mn_xSe$ is larger with larger x, the strain-induced shift correspondingly increasing for larger x. We report a direct observation of the longitudinal-optical phonon of MnSe in a MnSe/ZnTe MQW. Note that, in contrast to the wurtzite (rock-salt) structure possessed by $Cd_{1-x}Mn_xSe$ (MnSe) when grown in the bulk, these compounds assume the zinc-blende structure when fabricated by molecular-beam epitaxy (MBE), as in a MnSe/ZnTe MQW.[7]

II. EXPERIMENT

The MQW samples were grown on (100) GaAs substrates with ZnTe buffer layers, 2 μm thick for $ZnTe/Cd_{1-x}Mn_xSe$ and 0.5 μm thick for ZnTe/MnSe, using MBE. The details of the growth technique are described in Ref. 2. An optical cryostat incorporating superconducting coils for low-temperature measurements in the presence of a magnetic field was used to study the spin-flip Raman scattering. Raman spectra were excited with monochromatic lines from Kr^+ and Ar^+ lasers; the typical power for spin-flip measurements was less than 10 mW to prevent samples from being heated. A double monochromator and a standard photon-counting system were used to analyze and detect the scattered radiation. For Raman EPR (electron paramagnetic resonance) of Mn^{2+} the spectrometer was used in conjunction with a third monochromator, in order to achieve the requisite rejection of the parasitic radiation close to the laser frequency.

III. RESULTS AND DISCUSSIONS

A. Magnetic excitations

Figure 1 shows Stokes and anti-Stokes Raman lines observed in a $ZnTe/Cd_{1-x}Mn_xSe$ MQW, x=0.13, at temperature (T)=70 K, magnetic field (H)=60 kG, and exciting wavelength (λ_L)=6764 Å, the thicknesses of $Cd_{1-x}Mn_xSe$ and ZnTe being 28 Å and 160 Å, respectively. The peak at 5.6 cm^{-1} (labeled ω_{PM}) corresponds to Raman EPR, originating from transitions within the Zeeman multiplets of Mn^{2+}, having energies of $m_s g_{Mn^{2+}}\mu_B H$, where m_s is an integer, $g_{Mn^{2+}}$=2 is the g factor of Mn^{2+}, and μ_B is the Bohr magneton.[3] The peak around 30 cm^{-1} (labeled ω_{SFR}) is due to the spin-flip of electrons bound to donors.[8]

It is well known that the spin flip of electrons bound to donors in diluted magnetic semiconductors is greatly enhanced by the *s-d* exchange interaction between the *s*-like conduction-band electrons and the electrons in the

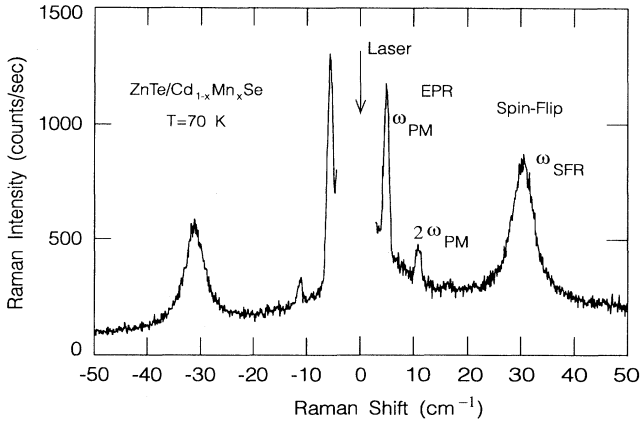

FIG. 1. Stokes and anti-Stokes components of Raman lines (electron paramagnetic resonance and spin-flip of donor-bound electrons) observed in $ZnTe/Cd_{1-x}Mn_xSe$ MQW's, x=0.13, at T=70 K, H=60 kG. Note that intensities of the anti-Stokes components are significantly higher than those expected from the Boltzmann factor, presumably due to the resonance condition under which the spectrum is taken.

d shell of Mn^{2+} ions. The spin-flip energy ($\hbar\omega_{SFR}$) consists of the intrinsic Zeeman splitting term and the *s-d* exchange term, namely,

$$\hbar\omega_{SFR} = \frac{\alpha}{g_{Mn^{2+}}\mu_B} M_0(H) + g^*\mu_B H, \quad (1)$$

where α is the exchange integral characterizing the *s-d* interaction, $M_0(H)$ is the macroscopic magnetization, and g^* is the intrinsic g factor. The exchange term is overwhelmingly larger than that determined by g^*, and from the magnetic-field dependence of the magnetization one can show that the spin-flip energy follows a Brillouin-function-like behavior given by

$$\hbar\omega_{SFR} = \tfrac{5}{2}\bar{x}\alpha N_0 B_{5/2}[g\mu_B H/k_B(T+T_{AF})], \quad (2)$$

where $\bar{x}$ is the effective manganese concentration[9] and T_{AF} is an antiferromagnetic temperature;[10] $\bar{x}$ and T_{AF} are phenomenological constants which take into account the antiferromagnetic interactions between Mn^{2+} ions, being introduced to fit the magnetization as a function of magnetic field at a given temperature. The selection rules for the spin-flip Raman scattering are discussed in detail in Ref. 8.

In Fig. 2 we show the spin-flip Raman shifts obtained from spectra such as the one shown in Fig. 1 as a function of magnetic field at several temperatures; also included are results obtained on bulk wurtzite $Cd_{1-x}Mn_xSe$, x=0.10,[8] as a function of magnetic field at various temperatures.[11] Our earlier study on the spin-flip Raman scattering in MBE-grown cubic $Cd_{1-x}Mn_xSe$ showed that the exchange integral α for a bulk grown crystal (with wurtzite structure) and that for a MBE-grown epilayer (with zinc-blende structure) agree within experimental error.[12] Thus the consistently smaller spin-flip Raman shift in the MQW's compared with that in the bulk can be attributed to the electron–wave-function

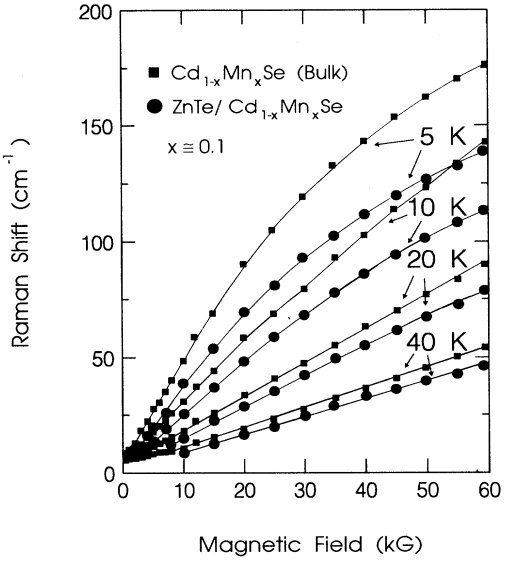

FIG. 2. Comparison of the Raman shifts associated with the spin-flip of donor-bound electrons in a wurtzite bulk $Cd_{1-x}Mn_xSe$ and in a $ZnTe/Cd_{1-x}Mn_xSe$ MQW for $x \sim 0.1$ at several temperatures.

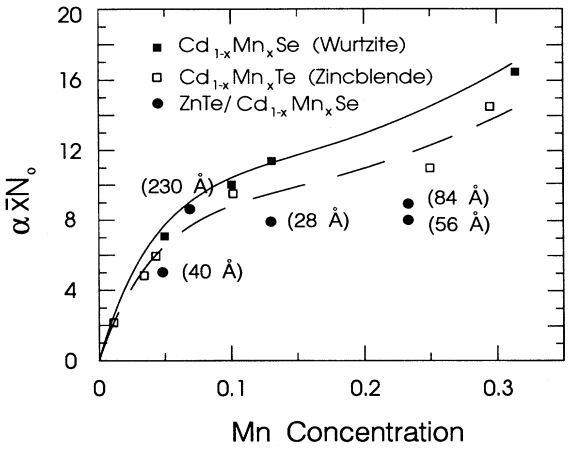

FIG. 3. The solid and dashed lines show the theoretical curve for $\alpha\bar{x}N_0$ vs Mn concentration in bulk $Cd_{1-x}Mn_xSe$ and $Cd_{1-x}Mn_xTe$, respectively. The solid and open squares are experimental values for bulk $Cd_{1-x}Mn_xSe$ and $Cd_{1-x}Mn_xTe$ samples, respectively. The values for $ZnTe/Cd_{1-x}Mn_xSe$ MQW's, shown as solid circles, are significantly smaller than those of the bulk samples of comparable Mn concentration. The well widths of the MQW's are indicated in the parentheses.

penetration into the nonmagnetic ZnTe barrier, i.e., the effective manganese concentration $\bar{x}$ "seen" by electrons in the MQW's is smaller than in the bulk for the same value of x. Note that the saturation of the Raman shift due to the saturation of the magnetization observed in the MQW's at low temperatures and at high fields is qualitatively similar to that observed in the bulk. This implies that the antiferromagnetic interaction between Mn^{2+} (as given by T_{AF}) with well width as narrow as 30 Å is comparable to that in the bulk alloy.

At low magnetic fields, the Brillouin function in Eq. (2) is linear in $H/(T+T_{AF})$ and a plot of $\left(\frac{\partial\hbar\omega_{SFR}}{\partial H}\right)^{-1}$ vs T is expected to be a straight line, the slope being proportional to $(\bar{x}\alpha N_0)^{-1}$. T_{AF} and $\bar{x}$ introduced in this context are constants appropriate for low temperatures. As in case of bulk (see Fig. 13 in Ref. 8), such a plot (not shown) is linear for $5 \leq T \leq 40$ K, but the slope as well as the value of $\left(\frac{\partial\hbar\omega_{SFR}}{\partial H}\right)^{-1}$ is larger than for the bulk of the corresponding Mn concentration. In Fig. 3 we show $\bar{x}\alpha N_0$ as a function of Mn^{2+} concentration, deduced from the slopes of such plots. The well widths of $Cd_{1-x}Mn_xSe$ are indicated in the figure. For comparison, the solid and open squares show the values for bulk $Cd_{1-x}Mn_xSe$ and $Cd_{1-x}Mn_xTe$, respectively, obtained from Ref. 8 in the same manner. The solid and dashed lines are theoretical fits of $\bar{x}\alpha N_0$, calculated from the value of αN_0 in bulk $Cd_{1-x}Mn_xSe$ =260 meV (Ref. 13) and in $Cd_{1-x}Mn_xTe$ =220 meV,[10] respectively, $\bar{x}$ being evaluated from the expression for $(\bar{x}/x)$ when $x \leq 0.05$, given in Ref. 9. The formula is developed by considering the probability of four types of nearest-neighbor Mn^{2+} clusters: singles, pairs, open triangles, and closed triangles for zinc-blende structure. For II-VI materials with the wurtzite structure the probabilities are the same except for the closed triangles, where the difference is insignificant for $x \leq 0.1$. It was shown that the theoretical values of $\bar{x}$ agree well with experimental data up to $x \leq 0.1$ for various II-VI DMS's. As seen in Fig. 3, it appears that the theoretical fit is good even up to $x \sim 0.3$. The values of $\bar{x}$ for the MQW's, however, are significantly smaller than for bulk samples, with $\bar{x}$ being smaller for narrower $Cd_{1-x}Mn_xSe$ wells. For a well width of 230 Å, $\bar{x}$ is very close to that for the bulk.

In Fig. 1 one can also clearly observe the Raman-EPR peaks at $\hbar\omega_{PM}$ and $2\hbar\omega_{PM}$. It has been argued earlier[3] that the selection rules for the Raman EPR as well as its resonance enhancement indicate that the Raman EPR is mediated by interband (or, equivalently, excitonic) transitions. In type-II superlattices, electrons are spatially separated from holes—and thus one may expect the Raman EPR mediated by interband transitions to be more difficult to observe. However, we have observed that both the magnetic and the vibrational Raman lines clearly increase in intensity when the excitation energy approaches the energy gaps reported in Fig. 1 of Ref. 4 as deduced from the reflectivity spectrum. We note here that these energies correspond to *spatially direct* transitions from quasibound states above the barrier for holes to the quantum confined electronic states, both localized in the $Cd_{1-x}Mn_xSe$ layer.[14]

B. Vibrational excitations

Depending on the boundary conditions relevant for the optical phonons of the constituent layers of a semiconductor superlattice, they may either freely propagate or be confined to one or the other constituent. If confined, features characteristic of the specific layer thick-

ness will manifest in the **q** vectors of the optical phonons observed in Raman scattering.[15] Acoustic vibrations of long wavelengths propagate freely through the superlattice and exhibit zone-folding effects associated with the larger period of the structure.[16] New Raman lines appear due to the zone folding consistent with the wave-vector conservation required in a light-scattering process. For a summary of various models for lattice dynamics of superlattices and for other types of vibrations in superlattices, e.g., interface mode, as well as for a detailed description of the optical and acoustic modes, we cite Ref. 17. In this section, we discuss confined optical modes, including the effect of strain due to the lattice mismatch between layers, and folded acoustic modes.

We have previously studied the zone-center optical phonon frequencies of MBE-grown cubic $Cd_{1-x}Mn_xSe$ ($x \leq 0.75$) epilayers and classified them as "MnSe-like" and "CdSe-like" since they follow a "two-mode" behavior.[12] As $x \rightarrow 1$, the CdSe-mode frequencies extrapolate to that of the gap mode of Cd^{2+} in zinc-blende MnSe and the MnSe-modes become the local mode of Mn^{2+} in CdSe. In contrast a ZnTe/CdSe superlattice is characterized by a single LO mode $\sim$210 cm^{-1}; this is consistent with the close proximity of the frequencies of the ZnTe and the CdSe zone-center LO phonon, at 209 and 212.6 cm^{-1}, respectively. One thus expects propagating optical phonons for this case. In Fig. 4, we show a spectrum obtained from a ZnTe/$Cd_{1-x}Mn_xSe$ MQW, x=0.23, the widths of the ZnTe and $Cd_{1-x}Mn_xSe$ layers being 84 Å and 160 Å, respectively, T=5 K, λ_L=6471 Å. The peak at 206.5 cm^{-1} corresponds to a *propagating* mode arising from the "CdSe-like" LO in the $Cd_{1-x}Mn_xSe$ layer and the ZnTe-LO in ZnTe, since both these zone-center optical phonons in the bulk occur $\sim$ 210 cm^{-1}. On the other hand the peak at 229.5 cm^{-1} corresponds to "MnSe-like" LO confined to the $Cd_{1-x}Mn_xSe$ layer, the arrow indicating the strain-free value expected for a $Cd_{1-x}Mn_xSe$ epilayer.

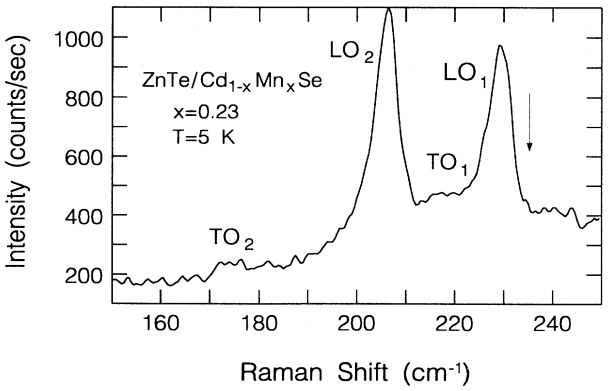

FIG. 4. Raman spectrum of the optical phonons in a ZnTe/$Cd_{1-x}Mn_xSe$ MQW, x=0.23. LO_1 and LO_2 correspond to a confined "MnSe-like" LO mode and a propagating mode (arising from "CdSe-like" and ZnTe LO phonons), respectively. The arrow indicates the strain-free value of "MnSe-like" LO frequency. "MnSe-like" TO and "CdSe-like" TO phonons are identified as TO_1 and TO_2, respectively.

"MnSe-like" LO frequencies in the MQW's are observed at lower frequencies than in the epilayers of $Cd_{1-x}Mn_xSe$, and the difference is the largest in a ZnTe/MnSe MQW, whose spectrum is shown in Fig. 5 with λ_L =5017 Å at T=5 K. The width of the MnSe layers is 33 Å and that of the ZnTe layers is 115 Å. MnSe LO is observed around 246 cm^{-1}, $\sim$11 cm^{-1} lower than the extrapolated value of the "MnSe-like" LO frequencies in $Cd_{1-x}Mn_xSe$, i.e., 257 cm^{-1} for x=1. We attribute this mainly to a strain-induced frequency shift and partly to the confinement of MnSe LO. There is an $\sim$3% lattice mismatch between ZnTe and MnSe, whereas the mismatch is only 0.4% between ZnTe and CdSe, resulting in the larger strain-induced shift in the phonon frequencies for the larger Mn concentration.

The strain-induced effect on optical phonons can be expressed as a superposition of a hydrostatic and a shear component. It can be shown that $\delta\omega_{LO} = \Delta\Omega_H + (2/3)\Delta\Omega$, where $\delta\omega_{LO}$ is the shift of the longitudinal-optical phonons and $\Delta\Omega_H$ and $\Delta\Omega$ are the shifts associated with the hydrostatic and shear components of the stress, respectively.[18] These shifts in turn are given by

$$\Delta\Omega_H = -2\gamma\omega_{LO}\frac{c_{11}-c_{12}}{c_{11}}\epsilon_\perp,$$

and (3)

$$\Delta\Omega = -\frac{p-q}{2\omega_{LO}}\frac{c_{11}+2c_{12}}{c_{11}}\epsilon_\perp,$$

where γ is the mode Grüneisen parameter, p and q are the deformation constants, c_{ij}'s are the elastic compliance constants, and $\epsilon_\perp$ is the strain in the plane perpendicular to the superlattice axis, given by $\epsilon_\perp = (a_\perp^{\text{eff}} - a_i)/a_i$. Here, $a_\perp^{\text{eff}}$ is the effective lattice constant in the plane, given by $a_\perp^{\text{eff}} = [n(a_1d_1 + a_2d_2) + a_Bd_B]/[n(d_1 + d_2) +$

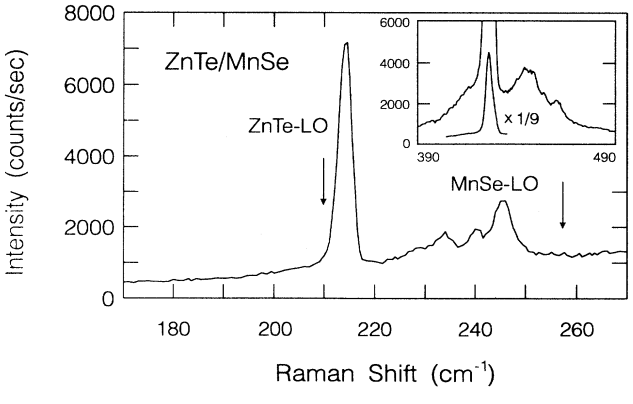

FIG. 5. Raman spectrum of the longitudinal-optical phonons in a ZnTe/MnSe MQW. The arrows indicate the strain-free values of ZnTe and MnSe LO-phonon frequencies. The inset shows two-phonon Raman spectrum corresponding to $2\omega_{LO}$(ZnTe) and ω_{LO}(ZnTe)+ω_{LO}(MnSe). The ZnTe LO phonons propagate through the superlattice, allowing their coupling with the confined MnSe LO phonons in the MnSe layer.

d_B],[19] where n is the number of periods and d's and a's with the subscripts 1, 2, and B are the layer thicknesses and the bulk lattice constants of the barrier, well, and buffer layers, respectively. For the results shown in Fig. 5, $\epsilon_\perp$ is 2.6% for the MnSe layer and –0.8% for the ZnTe layer. In the absence of the knowledge of the relevant parameters for MnSe, we assume them to be close to those of ZnSe, an approximation probably reasonable in view of the small mass difference between Mn and Zn. Thus, assuming the ZnSe values of γ=0.9, $(p-q)/2\omega_{LO}^2$=0.62,[21] $c_{11} = 9.29 \times 10^{10}$ N/m^2, and $c_{12} = 5.625 \times 10^{10}$ N/m^2,[22] respectively, we obtain $\delta\omega_{LO}$=–11 cm^{-1} for the MnSe LO phonons. Thus the shift of the experimentally observed MnSe LO from the extrapolated value of "MnSe-like" LO frequency in $Cd_{1-x}Mn_xSe$ epilayers appears to be predominantly strain-induced. One also expects a frequency shift of ZnTe-LO line in the opposite direction, although the shift is expected to be smaller due to the larger thickness of the ZnTe layers than that of the MnSe layers, as well as due to the presence of the ZnTe buffer layer. With γ=1.2,[21] $(p-q)/2\omega_{LO}^2$=0.6,[23] $c_{11} = 7.13 \times 10^{10}$ N/m^2, and $c_{12} = 4.07 \times 10^{10}$ N/m^2 (Ref. 24) for ZnTe, we obtain $\delta\omega_{LO}$=+3 cm^{-1}, in reasonable agreement with experimental results. For comparison, the ZnTe LO and MnSe LO frequencies in the bulk are shown by arrows in Fig. 5.

Although MnSe/ZnTe MQW's studied in this paper are highly strained, they display confined optical phonons as well as three pairs of folded acoustic phonons, testifying to their excellent structural quality. The peaks right below 250 cm^{-1} in Fig. 5 are the confined LO modes of MnSe, corresponding to $q_m = m\pi/(d_1 + a/2)$,[25] where m is an even integer and d_1 and a are the width and the lattice constant of MnSe, respectively. We note here that (001) superlattices have D_{2d} point-group symmetry and their long-wavelength optical phonons traveling along the superlattice axis belong either to the B_2 (m odd) or to the A_1 (m even) representations and, in resonance (especially when the scattered photon energy approaches a real electronic transition, i.e., in "out resonance") Raman effect, the A_1's dominate.[15] With λ_L=5145 Å, only one MnSe LO peak is found at 247.5 cm^{-1}, at a frequency higher than those in Fig. 5 with λ_L=5017 Å. We assign this to m=1 and the peaks in Fig. 5 to even m's. With this assignment, their measured frequencies are in good agreement with the dispersion curve calculated in the linear chain model for MnSe and shown in Fig. 6. In strained layers a variation in the Raman shift may be observed when the excitation energy is changed from below to above the band gap.[20] For the former, the laser light is transmitted, whereas for the latter light can penetrate only the skin depth. Thus the two experiments may probe different portions of the layers. In a ZnTe/MnSe MQW with a ZnTe buffer layer, one expects a larger strain in MnSe near the buffer layer than near the top surface, and the MnSe LO for λ_L=5145 Å is expected to be at a lower frequency. Since this is contrary to the experimental observation, we rule it out. Note that the Raman signal at $2\omega_{LO}$(ZnTe), shown in the inset, is ~5 times stronger than that at $1\omega_{LO}$(ZnTe). This indicates that the "out-resonance" condition is fulfilled more strongly for the overtone than for the fundamental mode, i.e., the energy of the scattered light $\omega_L - 2\omega_{LO}$ is more closely matched with interband transitions.[26]

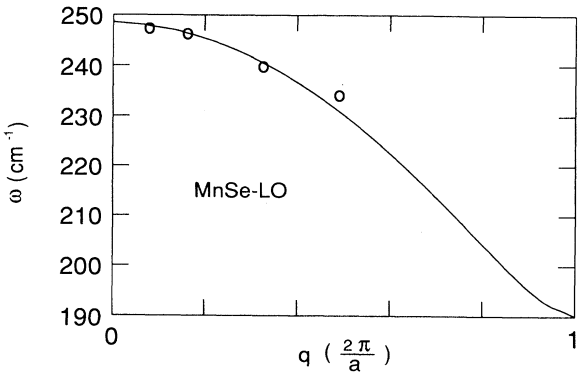

FIG. 6. The dispersion of MnSe LO phonons in strained MnSe obtained from the Raman shifts of confined MnSe LO$_m$ (m=1,2,4,6) in ZnTe/MnSe MQW's. Here, $q_m = m\pi/(d_1 + a/2)$. The curve is generated from the linear chain model with a spring constant adjusted to take into account the strain effect.

In the second-order Raman spectrum, the peak positions correspond to $2\omega_{LO}$(ZnTe) and ω_{LO}(ZnTe) + ω_{LO}(MnSe). It is somewhat surprising that a feature arising from a combination mode involving vibrational excitations *in two different layers* is observed in the Raman spectrum. We note that, in contrast to the confined MnSe LO, the ZnTe LO can propagate through the superlattice, since the dispersion curves originating from the two phonons overlap for frequencies equal to or smaller than the ZnTe LO at the zone center. Thus vibrations with frequencies corresponding to ZnTe LO and MnSe

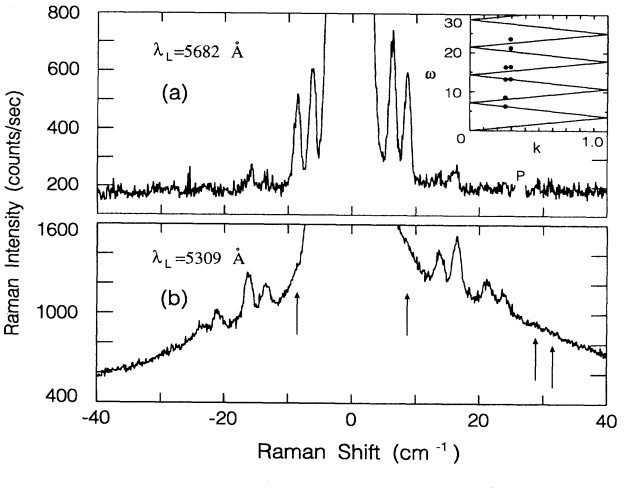

FIG. 7. Folded acoustic phonons in a ZnTe/MnSe MQW, with 5682 Å (a) and 5309 Å (b) excitation wavelengths. Arrows show positions for peaks that are reproducible though barely observable. P indicates a laser plasma line. In the inset, we show the dispersion of the longitudinal acoustic phonon in the MQW, i.e, the frequency (cm^{-1}) vs wave vector k in units of π/D. The dots are the experimental data obtained from the peak positions.

LO excitations can coexist in the MnSe layer, allowing a combination mode to be excited. It appears that a coupled mode associated with two constituent layers in this manner has not been previously reported.

The folded acoustic phonons observed in a ZnTe/MnSe superlattice are shown in Figs. 7(a) and 7(b), obtained at T=300 K with λ_L= 5682 Å and 5309 Å, respectively. (The widths of the MnSe and ZnTe layers are 65 Å and 115 Å, respectively.) Since the acoustic dispersion curves of the two constituent materials of the quantum-well structure overlap over a wide frequency range, acoustic phonons can propagate freely through both layers. The dispersion relation for the acoustic phonons propagating along the superlattice axis with wave vector q is then given by

$$\cos(qD) = \cos(\omega d_1/v_1)\cos(\omega d_2/v_2) - (1+\delta)\sin(\omega d_1/v_1)\sin(\omega d_2/v_2), \quad (4)$$

where $d_1(d_2)$, $\rho_1(\rho_2)$, and $v_1(v_2)$ are the thickness, density, and the sound velocity characterizing the barrier (the well), respectively, $D = d_1 + d_2$, and $\delta = \frac{1}{2}(\rho_1 v_1 - \rho_2 v_2)^2/(\rho_1 v_1 \rho_2 v_2)$.[16] From wave-vector conservation, one can show that the wave vector of the acoustic phonons is $4\pi n/\lambda_L$ in the backscattering geometry, where n is the refractive index and λ_L is the excitation wavelength. In the inset of Fig. 7, we show the dispersion calculated from the equation as well as the experimental data. Since the velocity of the LA phonon in MnSe is not known, we again assume c_{11} for MnSe to be close to that for ZnSe. From $c_{11} \sim 9\times10^{10}$ N/m^2 (Ref. 22) and ρ=4.326 g/cm^3, we have $v_1 = (c_{11}/\rho)^{1/2} \sim 4.6\times10^5$ cm/s. As can be seen, this rather crude approximation provides a surprisingly good fit to the experimental data.[27]

ACKNOWLEDGMENTS

We express our thanks to R. G. Alonso for his participation in some of the preliminary experiments. The work reported in this paper was carried out with support from the National Science Foundation, Grant No. DMR-89-21717 (A.K.R.) and from the Office of Naval Research, Grant No. N00014-90-J-1782 (J.K.F.).

[1] J. Ding, H. Jeon, A. V. Nurmikko, H. Luo, N. Samarth, and J. K. Furdyna, Appl. Phys. Lett. **57**, 2756 (1990); M. A. Haase, J. Qiu, J. M. DePuydt, and H. Cheng, Appl. Phys. Lett. **59**, 1272 (1991); W. Xie, D. C. Grillo, R. L. Gunshor, M. Kobayashi, G. C. Hua, N. Otsuka, H. Jeon, J. Ding, and A. V. Nurmikko, J. Vac. Sci. Technol. B **10**, 921 (1992).

[2] N. Samarth, H. Luo, A. Pareek, F. C. Zhang, M. Dobrowolska, J. K. Furdyna, W. C. Chou, A. Petrou, K. Mahalingam, and N. Otsuka, J. Vac. Sci. Technol. B **10**, 915 (1992).

[3] A. Petrou, D. L. Peterson, S. Venugopalan, R. R. Galazka, A. K. Ramdas, and S. Rodriguez, Phys. Rev. B **27**, 3471 (1983).

[4] D. D. Awschalom, M. R. Freeman, N. Samarth, H. Luo, and J. K. Furdyna, Phys. Rev. Lett. **66**, 1212 (1991).

[5] R. G. Alonso, Eunsoon Oh, A. K. Ramdas, H. Luo, N. Samarth, and J. K. Furdyna, Phys. Rev. B **44**, 8009 (1991).

[6] E.-K. Suh, D. U. Bartholomew, A. K. Ramdas, R. N. Bicknell, R. L. Harper, N. C. Giles, and J. F. Schetzina, Phys. Rev. B **36**, 9358 (1987).

[7] L. A. Kolodziejski, R. L. Gunshor, N. Otsuka, B. P. Gu, Y. Hefetz, and A. V. Nurmikko, Appl. Phys. Lett. **48**, 1482 (1986).

[8] D. L. Peterson, D. U. Bartholomew, U. Debska, A. K. Ramdas, and S. Rodriguez, Phys. Rev. B **32**, 323 (1985).

[9] Y. Shapira, S. Foner, D. H. Ridgley, K. Dwight, and A. Wold, Phys. Rev. B **30**, 4021 (1984).

[10] J. A. Gaj, R. Planel, and G. Fishman, Solid State Commun. **29**, 435 (1979).

[11] The magnetization of bulk $Cd_{1-x}Mn_xSe$ is larger for x=0.13 than for x=0.10 at $T \geq 5$ K, and thus the difference between the Raman shift in the bulk and in the MQW, both with x=0.13, is larger than that in Fig. 2.

[12] R. G. Alonso, Y. R. Lee, Eunsoon Oh, A. K. Ramdas, H. Luo, N. Samarth, J. K. Furdyna, and H. Pascher, Phys. Rev. B **43**, 9610 (1991).

[13] R. L. Aggarwal, S. N. Jasperson, J. Stankiewicz, Y. Shapira, S. Foner, B. Khazai, and A. Wold, Phys. Rev. B **28**, 6907 (1983).

[14] See results for analogous systems reported by F. C. Zhang, N. Dai, H. Luo, N. Samarth, M. Dobrowolska, J. K. Furdyna, and L. R. Ram-Mohan, Phys. Rev. Lett. **68**, 3220 (1992), and by H. Luo, N. Dai, F. C. Zhang, N. Samarth, M. Dobrowolska, J. K. Furdyna, C. Parks, and A. K. Ramdas (unpublished).

[15] A. K. Sood, J. Menendez, M. Cardona, and K. Ploog, Phys. Rev. Lett. **54**, 2111 (1985).

[16] C. Colvard, T. A. Gant, M. V. Klein, R. Merlin, R. Fischer, M. Morkoc, and A. C. Gossard, Phys. Rev. B **31**, 2080 (1985).

[17] B. Jusserand and M. Cardona, in *Light Scattering in Solids V*, edited by M. Cardona and G. Güntherodt, Topics in Applied Physics Vol. 66 (Springer-Verlag, New York, 1989), Chap. 3.

[18] F. Cerdeira, C. J. Buchenauer, F. H. Pollak, and M. Cardona, Phys. Rev. B **5**, 580 (1972); S. Venugopalan and A. K. Ramdas, *ibid.* **8**, 717 (1973).

[19] R. B. Bylsma, R. Frohne, J. Kossut, W. M. Becker, L. A. Kolodziejski, and R. L. Gunshor, in *Layered Structures and Epitaxy*, edited by J. M. Gibson, G. C. Osbourn, and R. M. Tromp, MRS Symposia Proceedings No. 56 (Materials Research Society, Pittsburgh, 1986), p. 223.

[20] D. J. Olego, K. Shahzad, J. Petruzzello, and D. Cammack, Phys. Rev. B **36**, 7674 (1987).

[21] Table 3.1 in Ref. 17.

[22] Landolt-Börnstein, New Series, Vol. 17b (Springer-Verlag, Berlin, 1982), p. 144. We used the value of c_{ij}'s at T=77 K for the confined optical phonon and c_{11} at T=300 K for the folded acoustic phonon.

[23] $(p-q)/2\omega_{LO}^2$ for ZnTe is not reported in the literature, and is estimated to be ~0.6 in J. Menendez, A. Pinczuk, J. P. Valladares, R. D. Feldman, and R. F. Austin, Appl. Phys. Lett. **50**, 1101 (1987). It is arbitrarily assumed to be 0.17 in

N. Pelekanos, Q. Fu, J. Ding, W. Walecki, A. V. Nurmikko, S. M. Durbin, J. Han, M. Kobayashi, and R. L. Gunshor, Phys. Rev. B **41**, 9966 (1990), yielding $\delta\omega_{LO}=+2$ cm^{-1}.

[24]Reference 22, p. 159.

[25]B. Jusserand and D. Paquet, Phys. Rev. Lett. **56**, 1752 (1986); A. K. Sood, J. Menendez, M. Cardona, and K. Ploog, *ibid.* **56**, 1753 (1986).

[26]Note that the band-gap energies of ZnTe and MnSe are 2.38 eV and 3.24 eV at 10 K, respectively. If the valence-band offset were close to that in ZnTe/CdSe, where the top of the ZnTe valence band is estimated to be about 600–700 meV above that of CdSe as deduced from the infrared absorption, one expects in ZnTe/MnSe a type-I alignment, i.e., ZnTe wells and MnSe barriers with a very small conduction-band offset.

[27]The experimental values are slightly higher than the theoretical ones; this could be due either to the layer thickness being somewhat thinner or v_1 being larger than estimated.